ЖЭТФ, 2007, том 131, вып. 5, стр. 908–921 

# PSEUDOGAP BEHAVIOR IN $Bi_2Ca_2SrCu_2O_8$: RESULTS OF GENERALIZED DYNAMICAL MEAN-FIELD APPROACH

***E. Z. Kuchinskii*** [a], ***I. A. Nekrasov*** [a], ***Z. V. Pchelkina*** [b], ***M. V. Sadovskii*** [a*]

[a] *Institute for Electrophysics, Russian Academy of Sciences*
*620016, Ekaterinburg, Russia*

[b] *Institute for Metal Physics, Russian Academy of Sciences*
*620219, Ekaterinburg, Russia*

Received 20 September 2006

Pseudogap phenomena are observed for the normal underdoped phase of different high-$T_c$ cuprates. Among others, the $Bi_2Sr_2CaCu_2O_{8-\delta}$ (Bi2212) compound is one of the most studied experimentally. To describe the pseudogap regime in Bi2212, we use a novel generalized *ab initio* LDA+DMFT+$\Sigma_{\mathbf{k}}$ hybrid scheme. This scheme is based on the strategy of one of the most powerful computational tools for real correlated materials: the local density approximation (LDA) + dynamical mean-field theory (DMFT). Conventional LDA+DMFT equations are here supplied with an additional (momentum-dependent) self-energy $\Sigma_{\mathbf{k}}$ in the spirit of our recently proposed DMFT+$\Sigma_{\mathbf{k}}$ approach accounting for pseudogap fluctuations. In the present model, $\Sigma_{\mathbf{k}}$ describes nonlocal correlations induced by short-range collective Heisenberg-like antiferromagnetic spin fluctuations. The effective single-impurity problem of the DMFT is solved by the numerical renormalization group (NRG) method. Material-specific model parameters for the effective $x^2-y^2$ orbital of Cu-$3d$ shell of the Bi2212 compound, e.g., the values of intra- and interlayer hopping integrals between different Cu sites, the local Coulomb interaction U, and the pseudogap potential $\Delta$ were obtained within the LDA and LDA+DMFT schemes. Here, we report the theoretical LDA+DMFT+$\Sigma_{\mathbf{k}}$ quasiparticle band dispersion and damping, Fermi surface renormalization, momentum anisotropy of (quasi) static scattering, densities of states, spectral densities, and angular-resolved photoemission (ARPES) spectra accounting for pseudogap and bilayer splitting effects for normal (slightly) underdoped Bi2212 ($\delta = 0.15$). We show that LDA+DMFT+$\Sigma_{\mathbf{k}}$ successfully describes strong (pseudogap) scattering close to Brillouin zone boundaries. Our calculated LDA+DMFT+$\Sigma_{\mathbf{k}}$ Fermi surfaces and ARPES spectra in the presence of pseudogap fluctuations are almost insensitive to the bilayer splitting strength. However, our LDA-calculated value of bilayer splitting is found to be rather small to describe the experimentally observed peak–dip–hump structure. The results obtained are in good semiquantitative agreement with various recent ARPES experiments.

PACS: 71.10.Fd, 71.10.Hf, 71.27.+a, 71.30.+h, 74.72.-h

## 1. INTRODUCTION

The pseudogap state is the major anomaly of the normal state of copper oxides, commonly believed to be most relevant for the understanding of the physical nature of high-$T_c$ superconductivity [1].

During the last decade, experimental techniques of angular-resolved photoemission spectroscopy (ARPES) have made an impressive progress. A state-of-the-art high-$T_c$ test compound for ARPES is the $Bi_2Sr_2CaCu_2O_{8-\delta}$ (Bi2212) system. A great amount of experimental ARPES data is therefore available for Bi2212 (see [2] for reviews). Several major experimental characteristics are derived from ARPES data, e.g., the Fermi surfaces (FS), quasiparticle band dispersions and damping, and even self-energy lineshapes [2]. A number of interesting physical anomalies were discovered in the normal underdoped phase of Bi2212: pseudogap formation, shadow bands, and bilayer splitting of the FS [2]. These phenomena abound in theories and there is still no definite point of view about their physical origin. It is believed that all of them are quite relevant to

*E-mail: sadovski@iep.uran.ru

the physics of high-temperature superconductors. The problem is greatly complicated by strong electronic correlations ever present in these compounds, making the standard band theory and Fermi-liquid approaches doubtful.

In this work, we show that accounting for the short-range antiferromagnetic fluctuations resulting in pseudogap formation together with bilayer splitting effects suffices, in principle, to describe the above-mentioned experiments. For this, we use a novel hybrid *ab initio* LDA+DMFT+$\Sigma_{\mathbf{k}}$ computational scheme [3–5]. On one hand, this scheme inherits all the advantages of LDA+DMFT [6–10], i.e., the merger of the first-principle one-electron density functional theory within the local density approximation (DFT/LDA) [11, 12] and the dynamical mean-field theory (DMFT) for strongly correlated electrons [13–17]. On the other hand, our scheme allows accounting for nonlocal correlation effects by introducing a momentum-dependent external self-energy preserving the conventional DMFT equations [3–5]. To solve the effective single-impurity problem of the DMFT, we here use the reliable numerical renormalization group (NRG) approach [18, 19].

This combined scheme is particularly suitable for describing electronic properties of real high-$T_c$ materials at finite doping in the normal state. First, all material-specific model parameters for the physically relevant effective $x^2 - y^2$ orbital of the Cu-3$d$ shell are obtained from LDA computations. Second, undoped cuprates are antiferromagnetic Mott insulators with $U \gg W$ (where $U$ is the value of the local Coulomb interaction and $W$ is the bandwidth of the noninteracting band), and therefore correlation effects are very important. Thus, at finite doping (up to the optimal doping), cuprates are typical strongly correlated metals. In our computational scheme, these strong electronic correlations are taken into account at the DMFT stage. To adapt LDA+DMFT to study the "antiferromagnetic" scenario of pseudogap formation in cuprates [1, 20–22], a $\mathbf{k}$-dependent self-energy $\Sigma_{\mathbf{k}}$ describing nonlocal correlations induced by (quasi) static short-ranged collective Heisenberg-like antiferromagnetic (AFM) spin fluctuations is included [21, 22].

Recently, we applied the DMFT+$\Sigma_{\mathbf{k}}$ approach to investigate the formation of a pseudogap for the strongly correlated metallic regime of the single-band Hubbard model on a square lattice [3–5]. At present, there are several independent methods aimed at describing nonlocal effects beyond the standard DMFT. Similar results about pseudogap formation in the two-dimensional Hubbard model were already obtained within the two-particle self-consistent approach [23], cluster DMFT extensions, such as the dynamical cluster approximation (DCA) [24, 25] and cellular DMFT (CDMFT) [23, 26–28], CPT [29–31], and via the model of two interacting Hubbard sites self-consistently embedded in a bath [32]. The EDMFT has been used to demonstrate pseudogap formation in the DOS due to dynamic Coulomb correlations [33]. Important progress was also made with weak-coupling approaches to the Hubbard model [34] and the functional renormalization group [35, 36]. In several papers, pseudogap formation was described in the framework of the $t$–$J$ model [37]. A more general scheme for the inclusion of nonlocal corrections was also formulated within the so-called GW extension to DMFT [38, 39]. A dynamical vertex approximation was proposed in [40] to study the Mott–Hubbard transition in the presence of nonlocal antiferromagnetic correlations. A Chain-DMFT extension was used to investigate the breakup of the Fermi surface near the Mott transition for the quasi-one-dimensional Hubbard model [41].

This paper is organized as follows. In Sec. 2, we present a short introduction to the *ab initio* self-consistent generalized combined LDA+DMFT+$\Sigma_{\mathbf{k}}$ scheme to account for short-range AFM correlations. Section 3 contains the Bi2212 material-specific information: the LDA calculated band structure and details on some model parameter calculations. The results and a discussion of LDA+DMFT+$\Sigma_{\mathbf{k}}$ computations for Bi2212 are presented in Secs. 4 and 5.

## 2. COMPUTATIONAL METHOD

### 1. Introducing a length scale into the DMFT: DMFT+$\Sigma_k$ approach

To introduce a spatial length scale into the conventional DMFT method [13–17], we recently proposed the generalized DMFT+$\Sigma_{\mathbf{k}}$ approach [3–5]. The main assumption of our approach is that the lattice and the Matsubara "time" Fourier transform of the single-particle Green's function can be written as

$$G(\omega, \mathbf{k}) = \frac{1}{i\omega + \mu - \varepsilon(\mathbf{k}) - \Sigma(\omega) - \Sigma_{\mathbf{k}}(\omega)}, \qquad (1)$$

where $\Sigma(\omega)$ is the local self-energy of DMFT and $\Sigma_{\mathbf{k}}(\omega)$ is some momentum-dependent part. Interference effects between these parts are neglected. An advantage of our generalized DMFT+$\Sigma_{\mathbf{k}}$ approach is the additive form of the self-energy in Eq. (1) [3–5]. It allows keeping the set of self-consistent equations of the standard DMFT [13–17]. But there are two distinctions.

First, at each DMFT iteration, we recalculate the corresponding $\mathbf{k}$-dependent self-energy $\Sigma_{\mathbf{k}}(\mu, \omega, [\Sigma(\omega)])$ within some (approximate) scheme, taking interactions with collective modes or order parameter fluctuations into account. Second, the local Green's function of the effective impurity problem is defined as

$$G_{ii}(\omega) = \frac{1}{N}\sum_{\mathbf{k}} \frac{1}{i\omega+\mu-\varepsilon(\mathbf{k})-\Sigma(\omega)-\Sigma_{\mathbf{k}}(\omega)}, \qquad (2)$$

at each step of the standard DMFT procedure.

Eventually, we obtain the sought Green's function in form (1), where $\Sigma(\omega)$ and $\Sigma_{\mathbf{k}}(\omega)$ are those appearing at the end of our iteration procedure.

To calculate $\Sigma_{\mathbf{k}}(\omega)$ for an electron moving in the random field of pseudogap fluctuations (assumed to be (quasi) static and Gaussian, which is valid at high enough temperatures [21, 22]) with dominant scattering momentum transfers of the order of the characteristic vector $\mathbf{Q} = (\pi/a, \pi/a)$ (where $a$ is the lattice spacing) of AFM fluctuations ("hot spot" model [1]), we use the recursion procedure proposed in Refs. [21, 22, 42]:

$$\Sigma_{\mathbf{k}}(\omega) = \Sigma_{n=1}(\omega, \mathbf{k}), \qquad (3)$$

where

$$\Sigma_n(\omega, \mathbf{k}) = \\ = \Delta^2 \frac{s(n)}{i\omega+\mu-\Sigma(\omega)-\varepsilon_n(\mathbf{k})+inv_n\kappa-\Sigma_{n+1}(\omega, \mathbf{k})}. \qquad (4)$$

The quantity $\Delta$ characterizes the pseudogap energy scale and $\kappa = \xi^{-1}$ is the inverse correlation length of short-range SDW fluctuations, $\varepsilon_n(\mathbf{k}) = \varepsilon(\mathbf{k}+\mathbf{Q})$, and $v_n = |v^x_{\mathbf{k}+\mathbf{Q}}| + |v^y_{\mathbf{k}+\mathbf{Q}}|$ for odd $n$, while $\varepsilon_n(\mathbf{k}) = \varepsilon(\mathbf{k})$ and $v_n = |v^x_{\mathbf{k}}| + |v^y_{\mathbf{k}}|$ for even $n$, with $v^{x,y}(\mathbf{p})$ determined by the usual momentum derivatives of the "bare" dispersion $\varepsilon(\mathbf{k})$, while $s(n)$ represents a combinatorial factor determining the number of Feynman diagrams [21, 22].

For the (Heisenberg) spin structure of the interaction with spin fluctuations in a "nearly antiferromagnetic Fermi-liquid" (the spin–fermion (SF) model in Ref. [21]), spin-conserving scattering processes obey commensurate combinatorics, while spin–flip scattering is described by diagrams of incommensurate type (the "charged" random field in Ref. [21]). In this model, the combinatorial factor $s(n)$ becomes [21]

$$s(n) = \begin{cases} \dfrac{n+2}{3} & \text{for odd } n, \\ \dfrac{n}{3} & \text{for even } n. \end{cases} \qquad (5)$$

Obviously, with this procedure, we introduce an important length scale $\xi$ not present in the conventional DMFT. Physically, this scale mimics the effect of short-range (SDW) fluctuations within the fermionic "bath" surrounding the effective Anderson impurity of the DMFT. We expect such a length-scale dependence to lead to a kind of competition between local and nonlocal physics.

Although we prefer to regard both parameters $\Delta$ and $\xi$ as phenomenological (to be determined by fitting experiments) [4], they can in principle be calculated from the microscopic model under consideration. For example, using the two-particle self-consistent approach in Refs. [23, 43] with the approximations introduced in Refs. [21, 22], we derived the following microscopic expression for $\Delta$ [4] within the standard Hubbard model:

$$\Delta^2 = U^2 \frac{\langle n_{i\uparrow} n_{i\downarrow}\rangle}{n^2} \langle (n_{i\uparrow} - n_{i\downarrow})^2\rangle, \qquad (6)$$

where we consider only scattering by antiferromagnetic spin fluctuations. The different local quantities — the total density $n$, the local densities $n_{i\uparrow}$ and $n_{i\downarrow}$, and the double occupancy $\langle n_{i\uparrow} n_{i\downarrow}\rangle$ — can easily be calculated within the standard DMFT [16]. A detailed derivation of (6) is given in Appendix B in Ref. [4]. The corresponding microscopic expressions for the correlation length $\xi = \kappa^{-1}$ can also be derived within the two-particle self-consistent approach [23, 43]. However, we expect these results for $\xi$ to be less reliable, because this approach is valid only for relatively small (or medium) values of $U/t$, as well as in the purely two-dimensional case, neglecting quasi-two-dimensional effects, which are obviously important for cuprates. Actually, our calculation experience shows that all the results obtained below are rather weakly dependent on the values of $\xi$ from the experimentally relevant [1] interval $(5\text{–}10)a$.

## 2. Bilayer splitting effects: the LDA+DMFT+$\Sigma_k$ formulation

To perform *ab initio* calculations for the Bi2212 system, we use the LDA+DMFT strategy proposed in Refs. [6–10]. The required bare band dispersion for the effective physically relevant Cu-3$d$ $x^2 - y^2$ orbital in the tight-binding representation is given by

$$\varepsilon(\mathbf{k}) = -2t(\cos k_x a + \cos k_y a) - 4t' \cos k_x a \cos k_y a - \\ - 2t''(\cos 2k_x a + \cos 2k_y a) - \\ - 2t'''(\cos k_x a \cos 2k_y a + \cos 2k_y a \cos k_y a), \qquad (7)$$

where $t$, $t'$, $t''$, and $t'''$ are hopping integrals within first four coordination spheres. The tight-binding equation for the interlayer dispersion is taken in the form

$$t_\perp(\mathbf{k}) = \frac{t_\perp}{4}(\cos k_x a - \cos k_y a)^2 \qquad (8)$$

given in Ref. [44] with the bilayer splitting equal to $2t_\perp$.

Because accounting for bilayer splitting (BS) effects in Bi2212 requires an essentially two-band model, we introduce the bare Hamiltonian in reciprocal space as the following matrix with respect to (bonding and antibonding) band indices:

$$\hat{\mathbf{H}}(\mathbf{k}) = \begin{pmatrix} \varepsilon(\mathbf{k}) & t_\perp(\mathbf{k}) \\ t_\perp(\mathbf{k}) & \varepsilon(\mathbf{k}) \end{pmatrix}. \quad (9)$$

The local Green's function is then also a matrix,

$$\hat{\mathbf{G}}(\omega) = \\ = \frac{1}{N}\sum_{\mathbf{k}} \left( i\omega - \hat{\mathbf{H}}(\mathbf{k}) - (\Sigma(\omega) + \Sigma_{\mathbf{k}}(\omega))\hat{\mathbf{I}} \right)^{-1}, \quad (10)$$

where we assume self-energies to be diagonal. In what follows, we keep the DMFT part of the problem just a single-band task. This can be achieved by taking the diagonal element of (10)

$$\widetilde{G}(\omega) = \frac{1}{N}\sum_{\mathbf{k}} \frac{G^{-1}(\omega,\mathbf{k})}{(G^{-1}(\omega,\mathbf{k}))^2 - (t_\perp(\mathbf{k}))^2}, \quad (11)$$

where $G(\omega,\mathbf{k})$ is given by (1). This local Green's function $\widetilde{G}(\omega)$ (which includes additive self-energy contributions) now determines our effective single-Anderson-impurity problem. We note that because we work with the single-band problem, there is no need for double-counting correction between LDA and DMFT [8].

## 3. LDA BAND STRUCTURE OF Bi2212 AND EFFECTIVE MODEL PARAMETERS

The Bi2212 compound has a tetragonal bcc crystal lattice with the symmetry space group $I4/mmm$ [45–47]. The main structural motif for this compound is two $CuO_2$ layers displaced close to each other in the unit cell. Using the crystal structure data in Ref. [45], we performed LDA calculations of the electronic band structure within the linearized muffin-tin orbital (LMTO) basis set [48]. The obtained band structure is in agreement with the one in Ref. [45].

In Fig. 1, the one-electron LDA band dispersion along BZ symmetry lines for Bi2212 is shown. Gray lines correspond to the all-band Hamiltonian. To extract the physically interesting partially filled $x^2-y^2$ orbital of Cu-3$d$ shell Wannier functions, the projecting method [49] in the LMTO framework [50] was applied. The corresponding dispersion of the effective $x^2-y^2$ orbital is displayed in Fig. 1 as the black line.

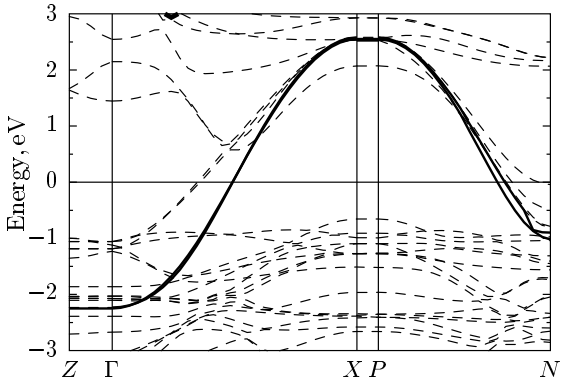


**Fig. 1.** Bi2212 band dispersions calculated within DFT+LDA (dashed lines) and the effective $x^2-y^2$ band of the Cu-3$d$ shell obtained by projection on Wannier functions (solid lines). The Fermi level corresponds to zero

Calculated energetic model parameters for Bi2212 (eV). The first four Cu-Cu inplain hopping integrals $t$, $t'$, $t''$, $t'''$, the interplain hopping value $t_\perp$, the local Coulomb interaction $U$, and the pseudogap potential $\Delta$

| $t$ | $t'$ | $t''$ | $t'''$ | $t_\perp$ | $U$ | $\Delta$ |
|---|---|---|---|---|---|---|
| −0.627 | 0.133 | 0.061 | −0.015 | 0.03 | 1.51 | 0.21 |

To set up the LDA+DMFT+$\Sigma_{\mathbf{k}}$ lattice problem (2), we must calculate the transfer integrals $t$, $t'$, $t''$, $t'''$, and $t_\perp$ for tight-binding expressions (7) and (8). On the basis of the Wannier function projecting method [49], we computed the corresponding hopping integrals with its LMTO realization [50]. The obtained values for intra- and interlayer hybridization between $x^2-y^2$ orbital of different Cu-sites are listed in the Table. The values of $t$, $t'$, $t''$, and $t'''$ we present are somewhat larger than those extracted from the ARPES experiment [51]. On the other hand, our value of $t_\perp$ is much smaller than the experimental one $t_\perp^{exp} = 0.083$ eV [51]. At the same time, our calculated value of $t_\perp$ is in good agreement with other band structure results reported in [52]. Taking the large difference between $t_\perp$ and $t_\perp^{exp}$ into account, we further provide LDA+DMFT+$\Sigma_{\mathbf{k}}$ results for both these values.

The value of the local Coulomb interaction $U$ for the $x^2-y^2$ orbital was obtained via the constrained LDA method [53]. To screen this $x^2-y^2$ orbital, we used the rest of the Cu-3$d$ shell of our selected site, the neighboring inplane Cu sites, and Cu sites from the closest $CuO_2$ layer. The value found is $U = 1.51$ eV

(see the Table).

The pseudogap potential $\Delta$ (see Eq. (6)) was obtained as described in Ref. [4] using LDA+DMFT(NRG) to calculate the set of occupancies entering (6) (instead of DMFT(QMC) used in Ref. [4]). For given values of hopping integrals and the $U$ value with the hole doping level $\delta = 0.15$, our $\Delta$ equals 0.21 eV. The value of the correlation length $\xi$ is always taken to be equal to 5 lattice constants, which is a typical experimental value [1]. Temperature enters through the NRG part of our scheme and is always taken to be about 255 K. This completes the set of necessary model parameters to start LDA+DMFT+$\Sigma_{\mathbf{k}}$ computations for Bi2212 (see Sec. 2).

## 4. RESULTS AND DISCUSSION

### 1. Bi2212 LDA+DMFT+$\Sigma_k$ densities of states

The density of states (DOS) is calculated as

$$N(\omega) = -\frac{1}{\pi}\,\mathrm{Im}\,\widetilde{G}(\omega), \tag{12}$$

where $\widetilde{G}(\omega)$ is defined by Eq. (11) analytically continued to real frequencies. In Fig. 2, we display the LDA+DMFT and LDA+DMFT+$\Sigma_{\mathbf{k}}$ DOS for the effective $x^2 - y^2$ orbital of Cu-3$d$. It is clearly seen that pseudogap fluctuations lead to formation of the pseudogap in the DOS within 0.2 eV from the Fermi level. In our model, this pseudogap is not tied to the Fermi level and it is not very pronounced for parameter values used here for Bi2212. It is also easy to find that for all our DOS curves, the BS effects are most pronounced on the top of the van Hove singularity, which is approximately $-0.2$ eV below the Fermi level (see the inset in Fig. 2 for details). Namely, we calculate the DOS for the LDA value of BS 0.03 eV (light curve) and the experimental BS value 0.083 eV (dark curve). For the latter, the BS effects are obviously stronger. Dashed curves correspond to LDA+DMFT results for two different values of bilayer splitting. For the LDA+DMFT+$\Sigma_{\mathbf{k}}$ DOS (solid curves), it is observed that BS effects become less pronounced (but can still be seen in the case of $t_\perp^{exp} = 0.083$ eV). This is caused by a decrease in the lifetime due to pseudogap fluctuations. Also, the van Hove singularity becomes slightly narrower here due to self-energy effects. We note that the shape of the pseudogap in the DOS is almost independent of the BS effects.

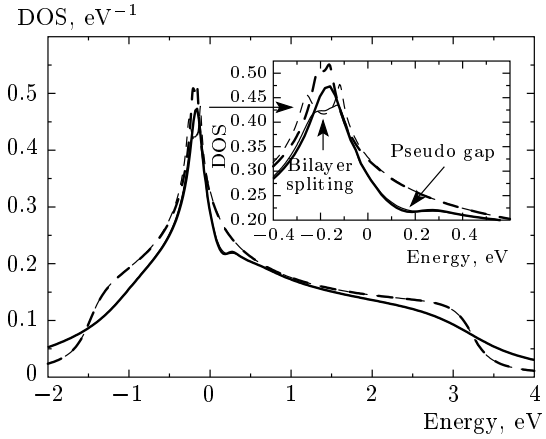


**Fig. 2.** The LDA+DMFT (dashed lines) and LDA+DMFT+$\Sigma_{\mathbf{k}}$ (solid lines) densities of states for Bi2212 for the LDA-calculated value $t_\perp = 0.03$ eV (dark curve) and the experimental value $t_\perp^{exp} = 0.083$ eV (light curve) (Coulomb interaction $U = 1.51$ eV, filling $n = 0.85$, pseudogap potential $\Delta = 0.21$ eV, correlation length $\xi = 5a$). The inset shows a magnified region around the Fermi level

### 2. Bi2212 LDA+DMFT+$\Sigma_k$ quasiparticle dispersions and damping

In the case of finite temperature and interaction values, we define quasiparticle dispersions via the positions of maxima of the corresponding spectral functions

$$A(\omega, \mathbf{k}) = -\frac{1}{\pi}\,\mathrm{Im}\,\widetilde{G}(\omega, \mathbf{k}), \tag{13}$$

where $\widetilde{G}(\omega, \mathbf{k})$ is defined by the summand in (11) analytically continued to real frequencies, with self-energies and the chemical potential $\mu$ calculated self-consistently as described in Sec. 2.1.

In Figs. 3 and 4, we present the LDA+DMFT and LDA+DMFT+$\Sigma_{\mathbf{k}}$ quasiparticle band dispersions (crosses) for the Bi2212 effective $x^2 - y^2$ orbital of the Cu-3$d$ shell along the symmetry lines in the Brillouin zone (BZ) for $t_\perp$ and $t_\perp^{exp}$. The background shows quasiparticle damping given by the imaginary part of the additive $\Sigma(\omega) + \Sigma_{\mathbf{k}}(\omega)$ self-energy. The more intensive shading corresponds to the larger damping. In the case of standard LDA+DMFT computations, with nonlocal corrections neglected (Fig. 3), one can clearly see that the damping is uniform over the entire BZ. This is due to the local nature of the conventional DMFT. Quasiparticles are well defined in a narrow light region around the zero energy (Fermi level).

When we introduce a spatial inhomogeneity into the DMFT bath within the LDA+DMFT+$\Sigma_{\mathbf{k}}$ approach, the damping turns out to be much stronger and consequently nonuniform, as can be seen in Fig. 4. Quasi-

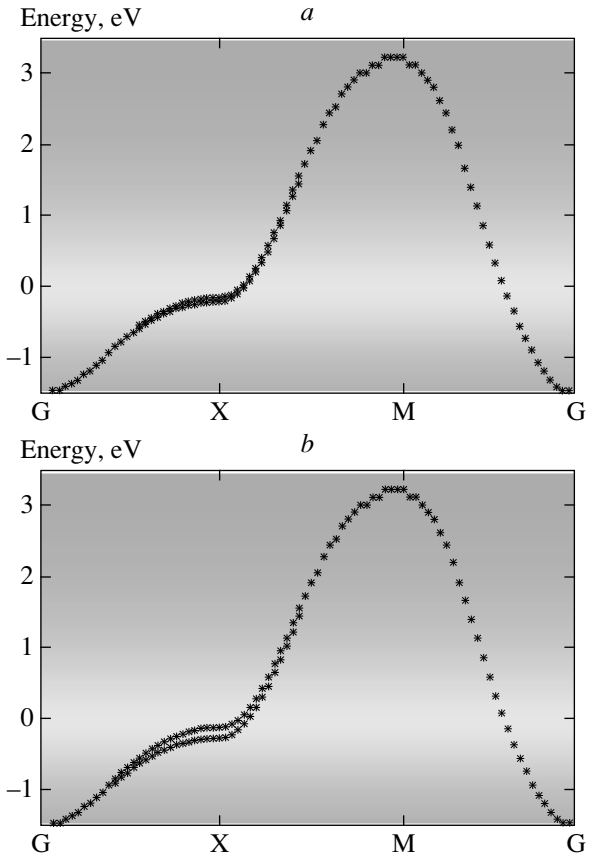


**Fig. 3.** The LDA+DMFT quasiparticle bands for Bi2212 (crosses) along the Brillouin zone high-symmetry directions for the LDA-calculated value $t_\perp = 0.03$ eV ($a$) and the experimental value $t_\perp^{exp} = 0.083$ eV ($b$) (Coulomb interaction $U = 1.51$ eV, filling $n = 0.85$). Zero of the background (which is $(1/\pi)\mathrm{Im}\,\Sigma(\omega)$, the local DMFT self-energy) corresponds to zero damping

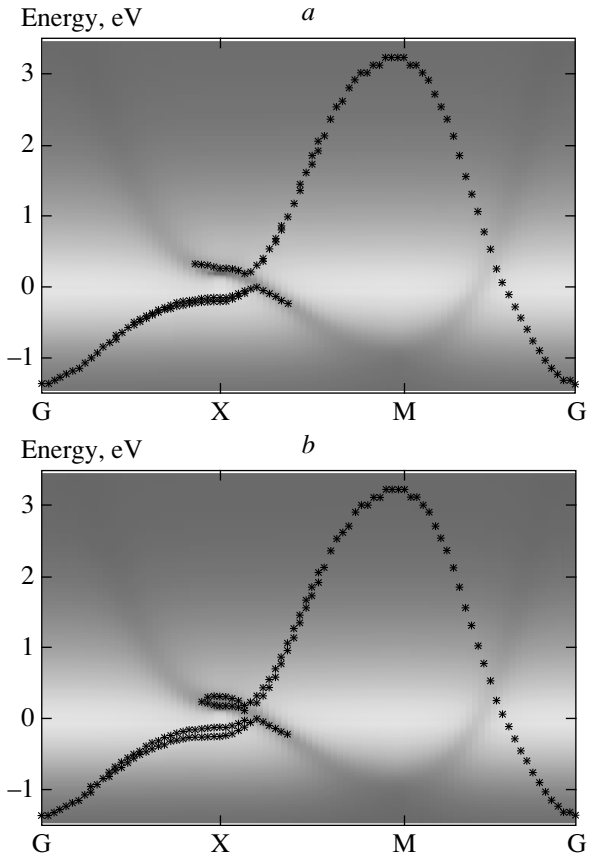


**Fig. 4.** The LDA+DMFT+$\Sigma_{\mathbf{k}}$ quasiparticle bands for Bi2212 (crosses) along the Brillouin zone high-symmetry directions for the LDA-calculated value $t_\perp = 0.03$ eV ($a$) and the experimental value $t_\perp^{exp} = 0.083$ eV ($b$) (Coulomb interaction $U = 1.51$ eV, filling $n = 0.85$, pseudogap potential $\Delta = 0.21$ eV, correlation length $\xi = 5a$). Zero of the background (which is $(1/\pi)\mathrm{Im}[\Sigma(\omega) + \Sigma_{\mathbf{k}}(\omega)]$, additive local and "pseudogap" self-energies) corresponds to zero damping

particles are again well defined close to the Fermi level. But now the contour plot of the $\mathrm{Im}[\Sigma(\omega) + \Sigma_{\mathbf{k}}(\omega)]$ self-energy (damping) clearly shows the so-called "shadow band", which looks like the quasiparticle band mirrored with respect to the zero energy. In Fig. 4, we can also see pseudogap formation around the X point. In our case, the shadow band is formed due to short-range AFM fluctuations. Close to the X point, BS effects are most pronounced. It can be seen that maxima of $A(\omega, \mathbf{k})$ belonging to the "shadow band" region are conserved only rather close to the X point and vanish due to large damping further away. In the middle of the MG direction, we observe preformation of an AFM insulating gap at the crossing point of the quasiparticle and "shadow" bands.

## 3. Bi2212 LDA+DMFT+$\Sigma_k$ spectral functions

To plot the spectral functions $A(\omega, \mathbf{k})$ in (13), we choose $\mathbf{k}$-points along the 1/8th part of the "bare" Fermi surface within the first quadrant of the Brillouin zone for given lattice spectra and filling. In Fig. 5, the corresponding spectral functions for different strength of bilayer splitting are shown.

Close to the nodal point (upper curve), the spectral function in Fig. 5 has a typical Fermi-liquid behavior, with a rather sharp peak close to the Fermi level. In going to the antinodal point (lower curve), fluctuations become stronger and push a sharp peak out of the Fermi level down in energy. Simultaneously with the growth of the fluctuation strength, damping

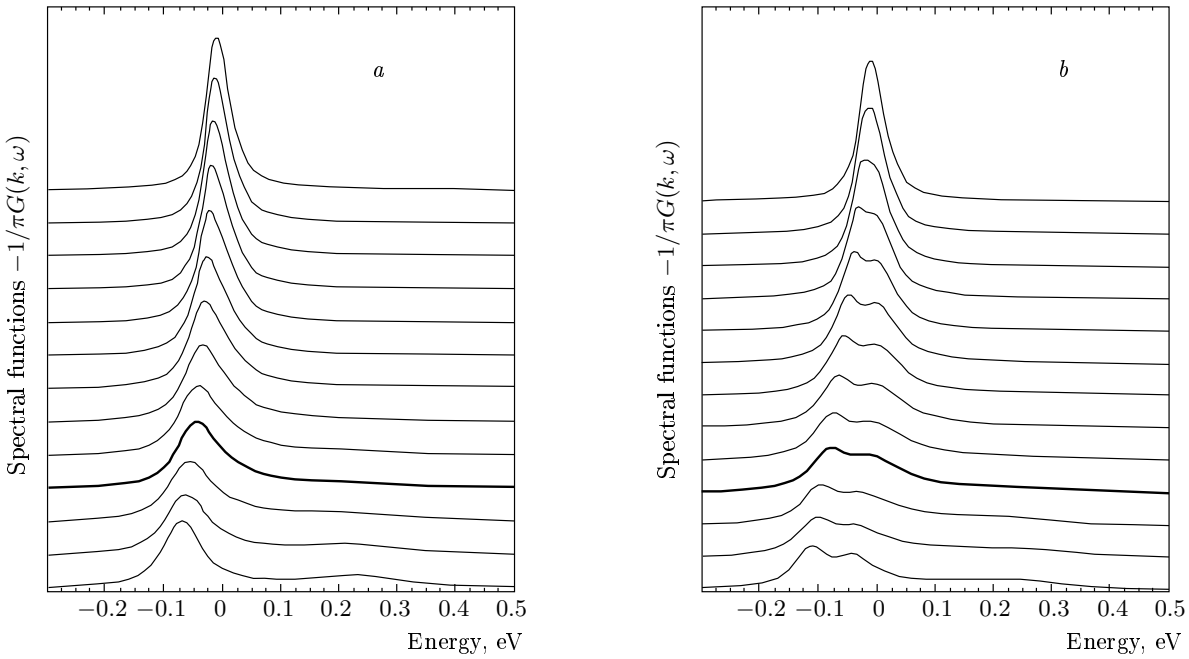


**Fig. 5.** The LDA+DMFT+$\Sigma_{\mathbf{k}}$ spectral densities for Bi2212 along the noninteracting Fermi surface in the 1/8th of the Brillouin zone for the LDA-calculated value $t_\perp = 0.03$ eV ($a$) and the experimental value $t_\perp^{exp} = 0.083$ eV ($b$) (Coulomb interaction $U = 1.51$ eV, filling $n = 0.85$, pseudogap potential $\Delta = 0.21$ eV, correlation length $\xi = 5a$)

also grows, and hence the peak becomes less intense and more broad. In the vicinity of the "hot spot" (solid line), the shape of $A(\omega, \mathbf{k})$ is completely modified: $A(\omega, \mathbf{k})$ becomes double-peaked and non-Fermi-liquid-like. Directly at the "hot spot", $A(\omega, \mathbf{k})$ has two peaks (the second one is much less intense) situated symmetrically with respect to the Fermi level and splitted from each other by approximately $1.5\Delta$ [21, 22].

In the case of $t_\perp^{exp}$ (Fig. 5$b$), behavior is similar to one for $t_\perp$ (Fig. 5$a$). However, the bilayer splitting strength is now big enough to be resolved, and hence a peak–dip–hump structure [2] is formed at the edges of the pseudogap.

## 4. Bi2212 LDA+DMFT+$\Sigma_k$ ARPES spectra

Knowing $A(\omega, \mathbf{k})$ in (13) of course allows us to calculate angle resolved photoemission (ARPES) spectra, which are the most direct experimental way to observe a pseudogap in real compounds. For that purpose, we only need to multiply our results for the spectral functions by the Fermi function at the temperature 255 K. The resulting LDA+DMFT+$\Sigma_{\mathbf{k}}$ ARPES spectra are presented in Fig. 6. They are again drawn along the 1/8th of the noninteracting FS from the antinodal (lower curve) to nodal point (upper curve). At the antinodal point, we find a well-defined (sharp) quasiparticle peak close to the Fermi level. In moving towards the antinodal point, the damping (widening) of this quasiparticle peak and its shift to higher binding energies are observed. Such behavior is typically obtained experimentally [2]. To describe the peak–dip–hump splitting resolved in experiment [2], we take $t_\perp^{exp} = 0.083$ eV [51]. Indeed, for $t_\perp^{exp}$, we obtain a pronounced peak–dip–hump structure similar to the experimental one [2]. It is recognized that our LDA-calculated $t_\perp$ is several times smaller and cannot provide an adequate description of the peak–dip–hump structure for ARPES data. We note that the intensity of the antibonding branch is higher than that of the bonding one. This is reversed in experiment. We attribute this difference to the matrix-element effects that are not taken into account in the present work.

In Fig. 7, we compare the LDA+DMFT+$\Sigma_{\mathbf{k}}$ ARPES spectra and the experimental one in Ref. [54] for Bi2212 measured along the Fermi surface. Here, the spectral functions displayed in Fig. 5 are multiplied by the Fermi function at the experimental temperature $T = 140$ K and convoluted with a Gaussian to simulate the experimental resolution of 16 meV [54]. All theoretical ARPES curves after multiplication and broadening are normalized to 1. Figure 7 corresponds to the theo-

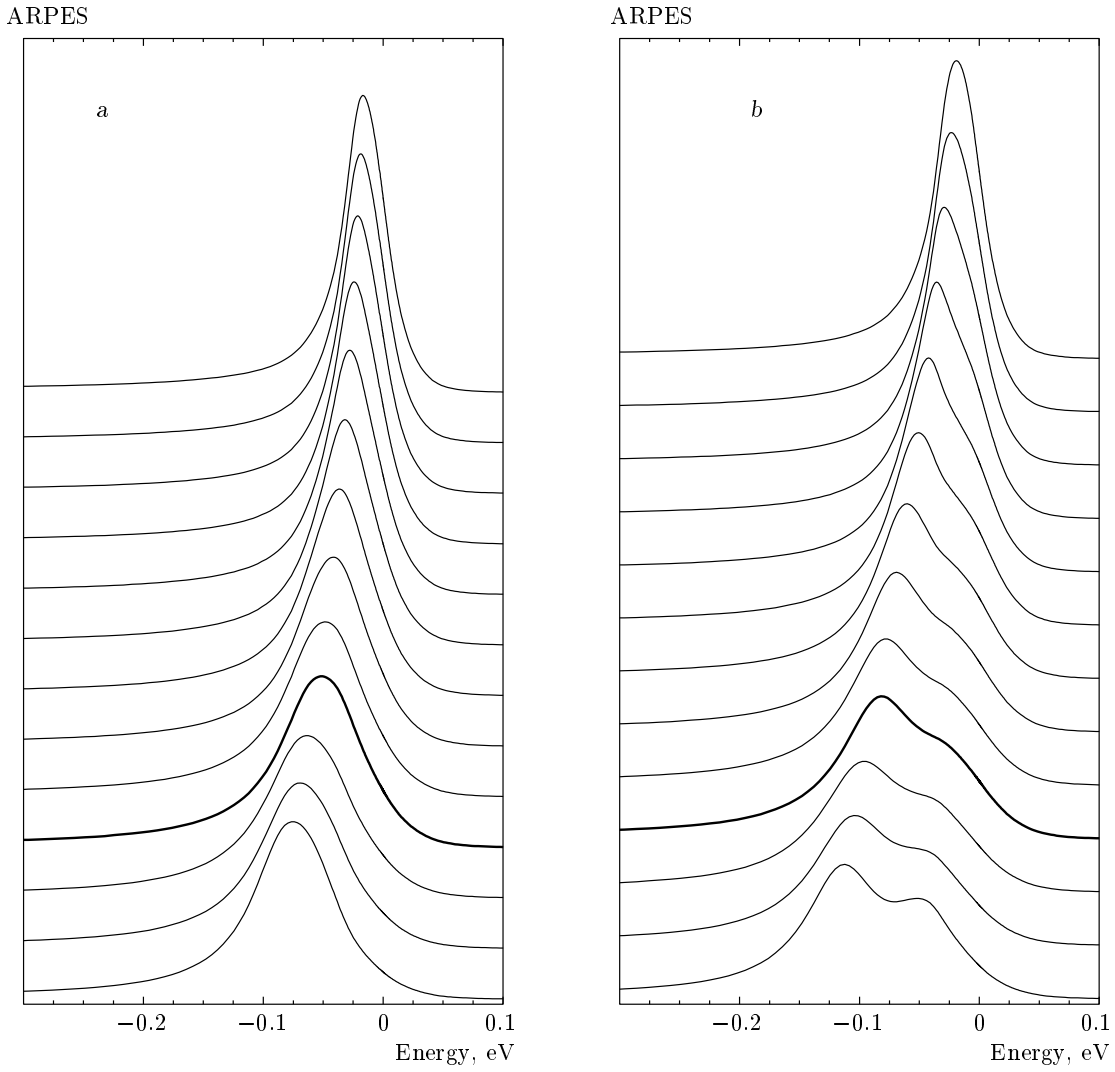


**Fig. 6.** The LDA+DMFT+$\Sigma_{\mathbf{k}}$ ARPES spectra for Bi2212 along the noninteracting Fermi surface in the 1/8th of the Brillouin zone for the LDA-calculated value $t_\perp = 0.03$ eV ($a$) and the experimental value $t_\perp^{exp} = 0.083$ eV ($b$). (Coulomb interaction $U = 1.51$ eV, filling $n = 0.85$, pseudogap potential $\Delta = 0.21$ eV, correlation length $\xi = 5a$.) The corresponding spectral function $A(\omega, \mathbf{k})$ is multiplied by the Fermi function at $T \sim 255$ K (the temperature of NRG calculations)

retical data for $t_\perp$ and $t_\perp^{exp}$ values. Both figures demonstrate a semiquantitative agreement of our theoretical results with the experiment. A common trend for both panels is the damping of the quasiparticle peak and its retreat to higher binding energies in moving from the nodal to the antinodal region. Displacements of theoretical and experimental peaks in Fig. 7$a$ are in a good quantitative agreement. But theoretical peaks are always a little bit sharper and narrower. We note that the left panel demonstrates no BS effects. In Fig. 7$b$, we found a slightly better agreement of intensities due to a larger BS value $t_\perp^{exp}$. But for the **k**-values between the "hot spot" and the antinodal point, we have some lack of spectral weight close to the Fermi level. Also for these **k**-values, we observe some reminiscence of the bilayer splitting. After all, we can infer that the BS effects do not change the line shape of our ARPES spectra significantly, and we obtain a rather satisfactory agreement with the experiment in both cases.

## 5. Bi2212 LDA+DMFT+$\Sigma_k$ Fermi surface

In what follows, we characterize the renormalized Fermi surfaces by intensity plots of the spectral density at zero frequency $A(\omega = 0, \mathbf{k})$ (which in the free-electron case just follow the "bare" Fermi surface).

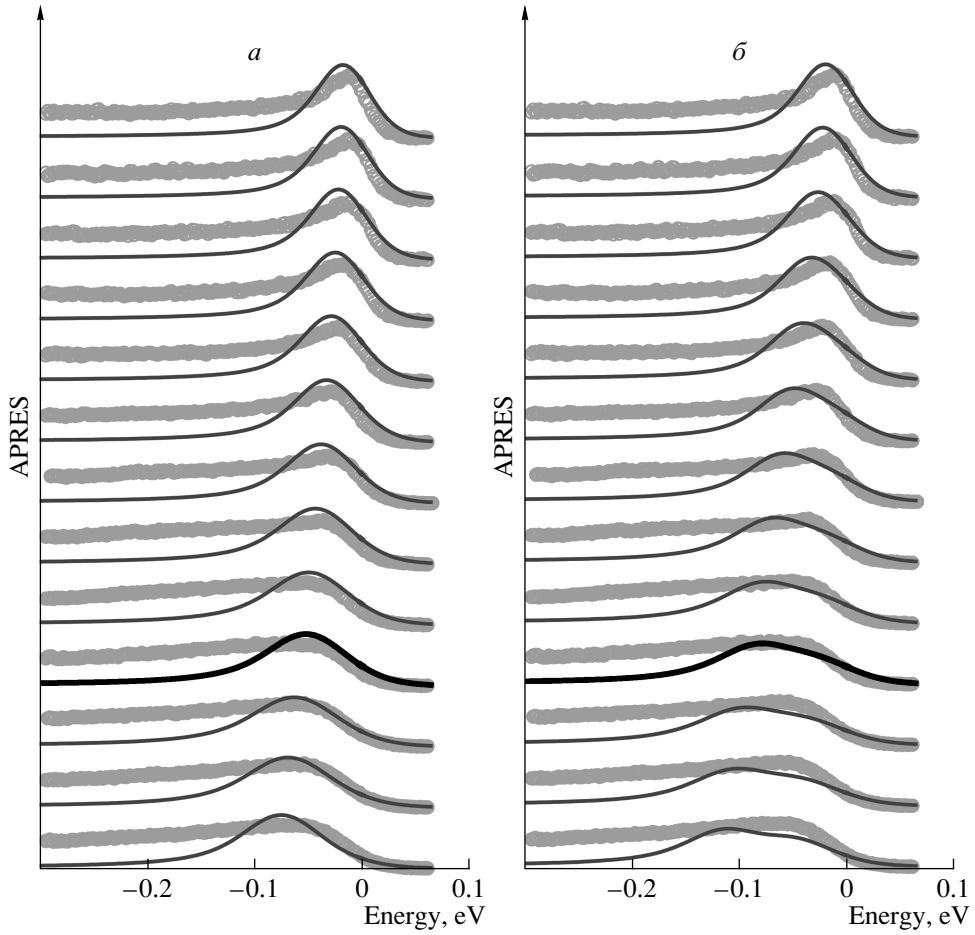


**Fig. 7.** Comparison of the LDA+DMFT+$\Sigma_{\mathbf{k}}$ ARPES spectra (solid lines) for Bi2212 along the noninteracting Fermi surface in the 1/8th of the Brillouin zone for the LDA-calculated value $t_\perp = 0.03$ eV ($a$) and the experimental value $t_\perp^{exp} = 0.083$ eV ($b$) with experimental ARPES (Ref. [54]) (circles). (Coulomb interaction $U = 1.51$ eV, filling $n = 0.85$, pseudogap potential $\Delta = 0.21$ eV, correlation length $\xi = 5a$.) The corresponding spectral function $A(\omega, \mathbf{k})$ is multiplied by the Fermi function at $T = 140$ K (the temperature of experiment) and broadened with a Gaussian to simulate the experimental resolution of 16 meV (Ref. [54])

In Figs. 8 and 9, we display the thus defined LDA+DMFT and LDA+DMFT+$\Sigma_{\mathbf{k}}$ Fermi surfaces for Bi2212. The LDA+DMFT FS has the LDA shape, as it should within the DMFT (see Fig. 8). Slight broadening close to the borders of the BZ is because of BS effects. A nonzero width of the FS (in contrast to the LDA) comes from a finite damping due to the interaction and temperature. For the LDA+DMFT+$\Sigma_{\mathbf{k}}$ FS (see Fig. 9), we see significant "destruction" effects in the vicinity of the antinodal point induced by pseudogap fluctuations. From comparison of the upper and lower panels in Fig. 9, we conclude that in the strongly correlated case, BS effects alone are not enough to describe the experimentally observed FS "destruction" close to the borders of the BZ and the formation of "Fermi arcs" around the nodal point, as observed in ARPES experiments [2]. We found that the shape of the Fermi surface is rather insensitive to the BS strength because pseudogap fluctuations are much stronger than the bilayer splitting and hide it. However, BS slightly amplifies pseudogap effects at the BZ boundaries. Thus, the account of pseudogap (AFM) fluctuations seems to be necessary to describe the experimental picture.

## 6. Bi2212 LDA+DMFT+$\Sigma_k$ anisotropy of static scattering

A strong anisotropy of (quasi) static scattering was observed in the Bi2212 system in ARPES experiments

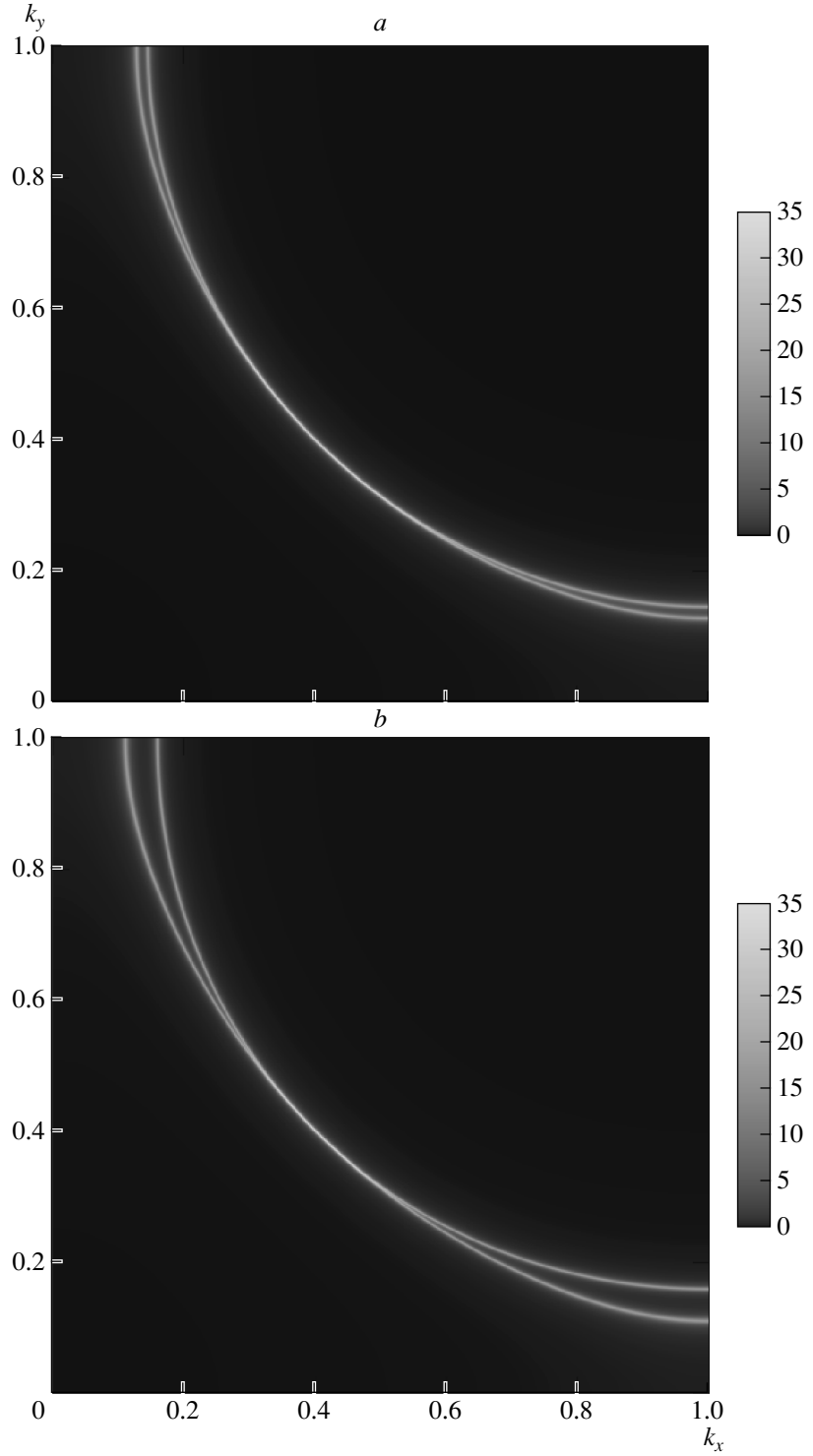


**Fig. 8.** The LDA+DMFT Fermi surfaces for Bi2212 within the $1/4$th of the Brillouin zone ($k_x$ and $k_y$ in units of $\pi/a$) for the LDA-calculated value $t_\perp = 0.03$ eV ($a$) and the experimental value $t_\perp^{exp} = 0.083$ eV ($b$) (Coulomb interaction $U = 1.51$ eV, filling $n = 0.85$)

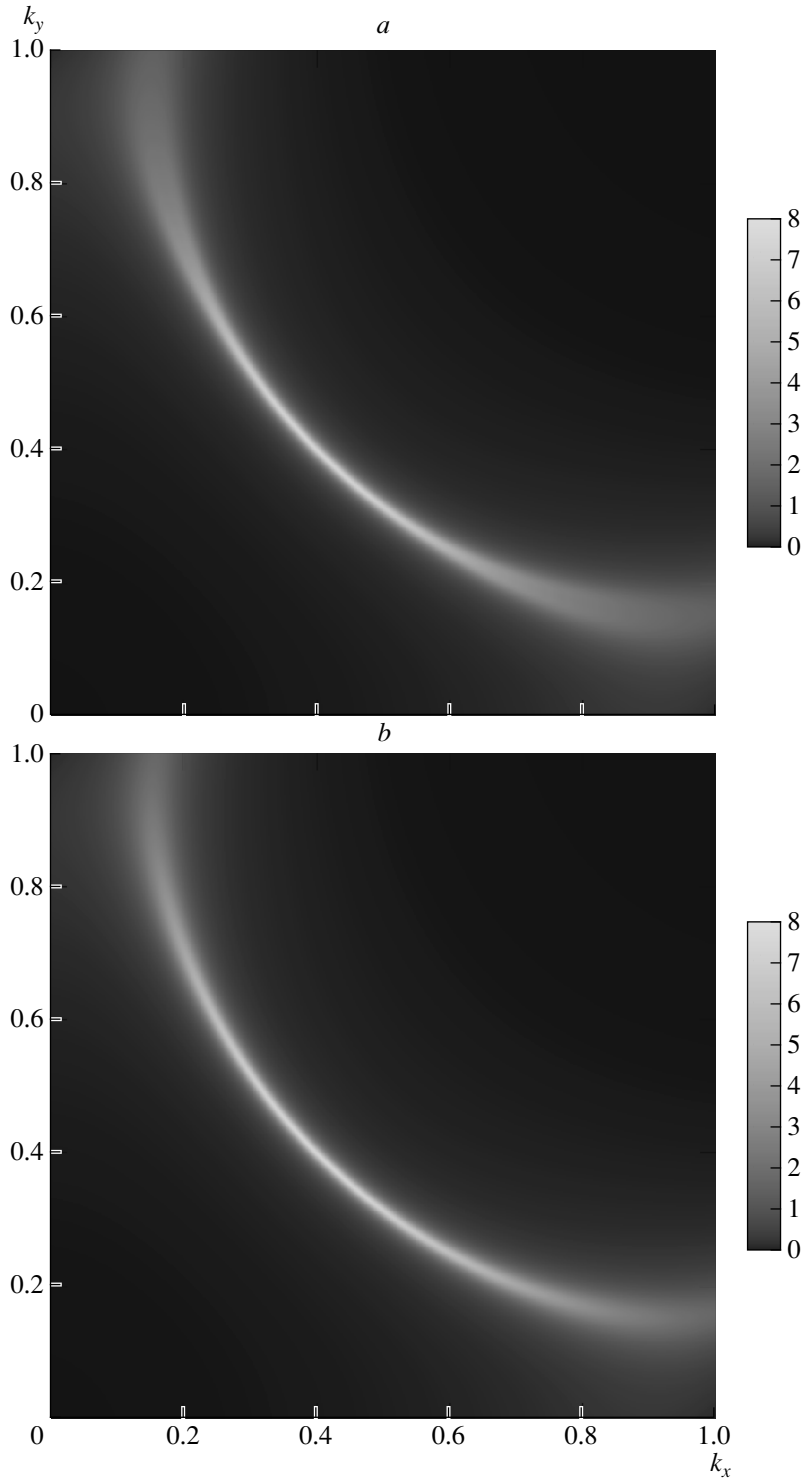


**Fig. 9.** The LDA+DMFT+$\Sigma_{\mathbf{k}}$ Fermi surfaces for Bi2212 within the $1/4$th of the Brillouin zone ($k_x$ and $k_y$ in inits of $\pi/a$) for the LDA-calculated value $t_\perp = 0.03$ eV ($a$) and the experimental value $t_\perp^{exp} = 0.083$ eV ($b$) (Coulomb interaction $U = 1.51$ eV, filling $n = 0.85$, pseudogap potential $\Delta = 0.21$ eV, correlation length $\xi = 5a$)

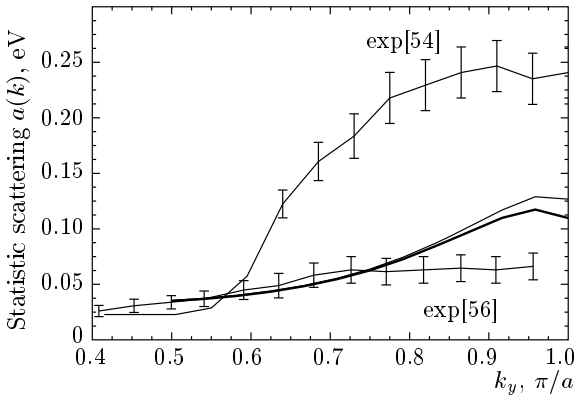


**Fig. 10.** Comparison of the experimental and theoretical LDA+DMFT+$\Sigma_{\mathbf{k}}$ static scattering $a(\mathbf{k}) = -(1/\pi)\,\mathrm{Im}\,\Sigma(0)+\Sigma_{\mathbf{k}}(0)$ for Bi2212 within the 1/8th of the Brillouin zone for the LDA-calculated value $t_\perp = 0.03$ eV (light curve) and the experimental value $t_\perp^{exp} = 0.083$ eV (dark curve) (Coulomb interaction $U = 1.51$ eV, filling $n = 0.85$, pseudogap potential $\Delta = 0.21$ eV, correlation length $\xi = 5a$)

in Refs. [54–56] and attributed to scattering by planar impurities [57, 58]. Here, we show that this effect can be naturally explained by (quasi) static scattering by pseudogap fluctuations.

Our LDA+DMFT+$\Sigma_{\mathbf{k}}$-calculated (quasi)static scattering defined as $a(\mathbf{k}) = \Sigma(0) + \Sigma_{\mathbf{k}}(0)$ is plotted in Fig. 10, together with the experimental data in Refs. [54, 56]. Here, $\mathbf{k}$-points are taken along the 1/8th of the noninteracting FS. We detect our results to mediate the experimental data in Refs. [54, 56], while the difference between these remains unexplained.

In our opinion, the anisotropy of (quasi)static scattering $a(\mathbf{k})$ naturally follows from the anisotropic renormalization of the electronic spectrum due to pseudogap fluctuations, which directly follows from our "hot spot"-like model [21, 22].

Although the overall behavior is analogous to the one obtained in the experiment, there is a need for further studies of the possible relevance of matrix-element effects in ARPES, as well as that of additional scattering by random static impurities [5].

## 5. CONCLUSION

The present investigation is aimed at describing the pseudogap regime of high-$T_c$ cuprate $Bi_2Sr_2CaCu_2O_{8-\delta}$ (Bi2212) from first principles. For this purpose, we used a novel generalized *ab initio* LDA+DMFT+$\Sigma_{\mathbf{k}}$ hybrid scheme. This scheme is based on the strategy of the most powerful computational tool for real correlated materials: the local density approximation (LDA) + dynamical mean-field theory (DMFT). We supply the conventional LDA+DMFT equations with an additional (momentum-dependent) self-energy $\Sigma_{\mathbf{k}}$ in the spirit of our recently proposed DMFT+$\Sigma_{\mathbf{k}}$ approach. The "external" self-energy $\Sigma_{\mathbf{k}}$ is then chosen to describe nonlocal dynamical correlations induced by short-range collective Heisenberg-like antiferromagnetic spin fluctuations (in the static Gaussian approximation in Refs. [21, 22]). Necessary Bi2212 material-specific model parameters for the effective $x^2 - y^2$ orbital of the Cu-3$d$ shell, e.g., the values of intra- and interlayer hopping integrals, the local Coulomb interaction $U$, and the pseudogap potential $\Delta$ were calculated within the LDA and LDA+DMFT. On the basis of LDA+DMFT+$\Sigma_{\mathbf{k}}$ computations, we obtain densities of states, the spectral functions $A(\omega, \mathbf{k})$ that allow visualizing the quasiparticle band dispersion and damping, the Fermi surface, the anisotropy of static scattering $a(\mathbf{k})$, and the ARPES spectra accounting for pseudogap and bilayer splitting effects for normal (slightly) underdoped Bi2212 ($\delta = 0.15$). It is found that on the DOS level, the BS and pseudogap effects are separated in energy and hardly affect each other. We showed that LDA+DMFT+$\Sigma_{\mathbf{k}}$ describes the strong scattering at the Brillouin zone boundaries as a pure many-body effect. The LDA+DMFT+$\Sigma_{\mathbf{k}}$ Fermi surface in the presence of pseudogap fluctuations is almost insensitive to the BS strength. Therefore, the BS effects alone are not enough to describe the Fermi surface destruction (although amplify it) and an additional source of electron scattering is required (for example, AFM short-range fluctuations). The only place where BS effects play a significant role is formation of the experimentally observed peak–dip–hump structure in ARPES spectra. The LDA-calculated value of bilayer splitting is found to be rather small to describe this effect. The results obtained are in a good semiqualitative agreement with various recent ARPES experiments.

At present, there are several alternative points of view on the possible explanation of the Fermi surface destruction, formation of shadow Fermi bands, etc. Recently, the analysis of the effect of three-dimensionality on the ARPES spectra was presented for Bi2212 in Ref. [59]. It was shown that in a quasi-two-dimensional system, the weak $k_z$-dispersion can lead to Fermi surface maps similar to those observed in the experiment. This Fermi-surface broadening mechanism does not have the many-body origin. The authors of Ref. [60]

have shown that the shadow Fermi surface in Bi2212 can be interpreted as an intrinsic feature of the initial electronic spectrum arising from bulk, orthorhombic distortions located primarily in the BiO planes, but most definitely felt throughout the three-dimensional crystal. All these effects are not considered here thus remain a subject of further investigations. Apparently, in a real system, these mechanisms combine with those described above leading to a complete picture of electronic structure of Bi2212.

We thank Thomas Pruschke for providing us with the NRG code. This work is supported by the RFBR grants 05-02-16301, 05-02-17244, 06-02-90537, the RAS programs "Quantum macrophysics" and "Strongly correlated electrons in semiconductors, metals, superconductors, and magnetic materials", the Dynasty Foundation, a Grant of the President of Russia MK.2118.2005.02, the interdisciplinary UB-SB RAS project, and the Russian Science Support Foundation.

## REFERENCES

1. T. Timusk and B. Statt, Rep. Progr. Phys, **62**, 61 (1999); M. V. Sadovskii, Usp. Fiz. Nauk **171**, 539 (2001).

2. A. Damascelli, Z. Hussain, and Z.-X. Shen, Rev. Mod. Phys. **75**, 473 (2003); J. C. Campuzano, M. R. Norman, and M. Randeria, in *Physics of Superconductors*, Vol. II, ed. by K. H. Bennemann and J. B. Ketterson, Springer, Berlin (2004), p. 167; J. Fink et al., E-print archives, cond-mat/0512307; X. J. Zhou et al., E-print archives, cond-mat/0604284.

3. E. Z. Kuchinskii, I. A. Nekrasov, and M. V. Sadovskii, JETP Lett. **82**, 198 (2005).

4. M. V. Sadovskii, I. A. Nekrasov, E. Z. Kuchinskii, Th. Prushke, and V. I. Anisimov, Phys. Rev. B **72**, 155105 (2005).

5. E. Z. Kuchinskii, I. A. Nekrasov, and M. V. Sadovskii, Low Temp. Phys. **32**, 528 (2006).

6. V. I. Anisimov, A. I. Poteryaev, M. A. Korotin, A. O. Anokhin, and G. Kotliar, J. Phys.: Condens. Matter **9**, 7359 (1997).

7. A. I. Lichtenstein and M. I. Katsnelson, Phys. Rev. B **57**, 6884 (1998).

8. I. A. Nekrasov, K. Held, N. Blümer, A. I. Poteryaev, V. I. Anisimov, and D. Vollhardt, Europhys. J. B **18**, 55 (2000).

9. K. Held, I. A. Nekrasov, G. Keller, V. Eyert, N. Blumer, A. K. McMahan, R. T. Scalettar, Th. Pruschke, V. I. Anisimov, and D. Vollhardt, Psi-k Newsletter **56**, 65 (2003) [psi-k.dl.ac.uk/newsletters/News_56/Highlight_56.pdf].

10. K. Held, I. A. Nekrasov, N. Blümer, V. I. Anisimov, and D. Vollhardt, Int. J. Mod. Phys. B **15**, 2611 (2001); K. Held, I. A. Nekrasov, G. Keller, V. Eyert, N. Blümer, A. K. McMahan, R. T. Scalettar, T. Pruschke, V. I. Anisimov, and D. Vollhardt, in *Quantum Simulations of Complex Many-Body Systems: From Theory to Algorithms*, ed. by J. Grotendorst, D. Marks, and A. Muramatsu, NIC Series Vol. 10 (NIC Directors, Forschunszentrum Jülich, 2002) p. 175; A. I. Lichtenstein, M. I. Katsnelson, and G. Kotliar, in *Electron Correlations and Materials Properties, 2nd ed.*, ed. by A. Gonis, Nicholis Kioussis, and Mikael Ciftan, Kluwer Academic/Plenum, New York (2002), p. 428.

11. W. Kohn and L. J. Sham, Phys. Rev. **140**, A1133 (1965); L. J. Sham and W. Kohn, Phys. Rev. **145**, 561 (1966).

12. L. Hedin and B. I. Lundqvist, J. Phys. C **4**, 2064 (1971); U. von Barth and L. Hedin, J. Phys. C **5**, 1629 (1972).

13. W. Metzner and D. Vollhardt, Phys. Rev. Lett. **62**, 324 (1989).

14. D. Vollhardt, in *Correlated Electron Systems*, ed. by V. J. Emery, World Scientific, Singapore (1993), p. 57.

15. Th. Pruschke, M. Jarrell, and J. K. Freericks, Adv. Phys. **44**, 187 (1995).

16. A. Georges, G. Kotliar, W. Krauth, and M. J. Rozenberg, Rev. Mod. Phys. **68**, 13 (1996).

17. G. Kotliar and D. Vollhardt, Phys. Today **57**, № 3, 53 (2004).

18. K. G. Wilson, Rev. Mod. Phys. **47**, 773 (1975); H. R. Krishna-murthy, J. W. Wilkins, and K. G. Wilson, Phys. Rev. B **21**, 1003 (1980); **21**, 1044 (1980); A. C. Hewson, *The Kondo Problem to Heavy Fermions*, Cambridge University Press (1993).

19. R. Bulla, A. C. Hewson, and Th. Pruschke, J. Phys.: Condens. Matter **10**, 8365 (1998);

20. D. Pines, E-print archives, cond-mat/0404151.

21. J. Schmalian, D. Pines, and B. Stojkovic, Phys. Rev. B **60**, 667 (1999).

22. E. Z. Kuchinskii and M. V. Sadovskii, Zh. Eksp. Teor. Fiz. **115**, 1765 (1999).

**23**. A.-M. S. Tremblay, B. Kyung, and D. Senechal, Low Temp. Phys. **32**, 561 (2006).

**24**. Th. Maier, M. Jarrell, Th. Pruschke, and M. Hettler, Rev. Mod. Phys. **77**, 1027 (2005).

**25**. Th. A. Maier, Th. Pruschke, and M. Jarrell, Phys. Rev. B **66**, 075102 (2002).

**26**. G. Kotliar, S. Y. Savrasov, G. Palsson, and G. Biroli, Phys. Rev. Lett. **87**, 186401 (2001); M. Capone, M. Civelli, S. S. Kancharla, C. Castellani, and G. Kotliar, Phys. Rev. B **69**, 195105 (2004).

**27**. B. Kyung, S. S. Kancharla, D. Senechal, A.-M. S. Tremblay, M. Civelli, and G. Kotliar, E-print archives, cond-mat/0502565.

**28**. M. Civelli, M. Capone, S. S. Kancharla, O. Parcollet, and G. Kotliar, E-print archives, cond-mat/0411696.

**29**. C. Gros and R. Valenti, Ann. der Phys. **3**, 460 (1994).

**30**. D. Senechal, D. Perez, and M. Pioro-Ladrie, Phys. Rev. Lett. **84**, 522 (2000); D. Senechal, D. Perez, and D. Plouffe, Phys. Rev. B **66**, 075129 (2002).

**31**. D. Senechal and A.-M. S. Tremblay, Phys. Rev. Lett. **92**, 126401 (2004).

**32**. T. D. Stanescu and P. Phillips, Phys. Rev. Lett. **91**, 017002 (2003).

**33**. K. Haule, A. Rosch, J. Kroha, and P. Wölfle, Phys. Rev. Lett. **89**, 236402 (2002); Phys. Rev. B **68**, 155119 (2003).

**34**. B. Kyung, V. Hankevich, A.-M. Dare, and A.-M. S. Tremblay, Phys. Rev. Lett. **93**, 147004 (2004).

**35**. A. A. Katanin and A. P. Kampf, Phys. Rev. Lett. **93**, 106406 (2004).

**36**. D. Rohe and W. Metzner, Phys. Rev. B **71**, 115116 (2005).

**37**. P. Prelovsek and A. Ramsak, Phys. Rev. B **63**, 180506 (2001); P. Prelovsek, and A. Ramsak, E-print archives, cond-mat/0502044.

**38**. S. Biermann, F. Aryasetiawan, and A. Georges, Phys. Rev. Lett. **90**, 086402 (2003).

**39**. P. Sun and G. Kotliar, Phys. Rev. Lett. **92**, 196402 (2004).

**40**. A. Toschi, A. A. Katanin, and K. Held, E-print archives, cond-mat/0603100.

**41**. C. Berthod, T. Giamarchi, S. Biermann, and A. Georges, E-print archives, cond-mat/0602304.

**42**. M. V. Sadovskii, Zh. Eksp. Teor. Fiz. **77**, 2070 (1979).

**43**. Y. M. Vilk and A.-M. S. Tremblay, J. de Phys. **7**, 1309 (1997).

**44**. O. K. Andersen, A. I. Liechtenstein, O. Jepsen, and F. Paulsen, J. Phys. Chem. Sol. **56**, 1573 (1995).

**45**. M. Hybertsen and L. Mattheiss, Phys. Rev. Lett. **60**, 1661 (1988).

**46**. J. M. Tarascon et al., Phys. Rev. B **37**, 9382 (1988).

**47**. S. A. Sunshine et al., Phys. Rev. B **38**, 893 (1988).

**48**. O. K. Anderson, Phys. Rev. B **12**, 3060 (1975); H. L. Skriver, *The LMTO Method*, Springer-Verlag, New York (1984).

**49**. N. Marzari and D. Vanderbilt, Phys. Rev. B **56**, 12847 (1997); W. Ku et al., Phys. Rev. Lett. **89**, 167204 (2002).

**50**. V. I. Anisimov et al., Phys. Rev. B **71**, 125119 (2005).

**51**. A. A. Kordyuk, S. V. Borisenko, M. Knupfer, and J. Fink, Phys. Rev. B **67**, 064504 (2003).

**52**. A. A. Kordyuk, S. V. Borisenko, A. N. Yaresko, S.-L. Drechsler, H. Rosner, T. K. Kim, A. Koitzsch, K. A. Nenkov, M. Knupfer, J. Fink, R. Follath, H. Berger, B. Keimer, S. Ono, and Yoichi Ando, Phys. Rev. B **70**, 214525 (2004).

**53**. O. Gunnarsson, O. K. Andersen, O. Jepsen, and J. Zaanen, Phys. Rev. B **39**, 1708 (1989).

**54**. A. Kaminski, H. M. Fretwell, M. R. Norman, M. Randeria, S. Rosenkranz, J. C. Campuzano, J. Mesot, T. Sato, T. Takahashi, T. Terashima, M. Takano, K. Kadowaki, Z. Z. Li, and H. Raffy, Phys. Rev. B **71**, 014517 (2005).

**55**. T. Valla, A. V. Fedorov, P. D. Johnson, Q. Li, G. D. Gu, and N. Koshizuka, Phys. Rev. Lett. **85**, 828 (2000).

**56**. A. Kaminski, H. M. Fretwell, M. R. Norman, M. Randeria, S. Rosenkranz, J. C. Campuzano, J. Mesot, T. Sato, T. Takahashi, T. Terashima, M. Takano, K. Kadowaki, Z. Z. Li, and H. Raffy, E-print archives, cond-mat/0404385.

**57**. C. M. Varma and E. A. Abrahams, Phys. Rev. Lett. **86**, 4652 (2001).

**58**. E. Abrahams and C. M. Varma, Proc. Nat. Acad. Sci. USA **97**, 5714 (2000).

**59**. A. Bansil, M. Lindroos, S. Sahrakorpi, and R. S. Markiewicz, Phys. Rev. B **71**, 012503 (2005).

**60**. A. Mans, I. Santoso, Y. Huang, W. K. Siu, S. Tavaddod, V. Arpiainen, M. Lindroos, H. Berger, V. N. Strocov, M. Shi, L. Patthey, and M. S. Golden, Phys. Rev. Lett. **96**, 107007 (2006).